

Review

# A Review on Biomedical MIMO Radars for Vital Sign Detection and Human Localization

Emanuele Cardillo \* and Alina Caddemi

Department of Engineering, University of Messina, 98166 Messina, Italy; academ@unime.it

\* Correspondence: ecardillo@unime.it; Tel.: +39-003-090-6765388

Received: 24 August 2020; Accepted: 8 September 2020; Published: 11 September 2020



**Abstract:** This paper reports a thorough overview on the last developments concerning the vital sign detection and the human localization employing the multiple-input-multiple-output (MIMO) technology. The wireless motion and vital sign detection represents an outstanding research area aimed at monitoring the health conditions of human subjects and at detecting their presence in different environments with minimal concern. MIMO radars exhibit several interesting advantages over conventional single-input-single-output architectures mainly related to their angle detection capabilities and enhanced signal-to-noise ratio. This paper describes the main features and details the operating principles of MIMO technology. Thereafter, it summarizes the state-of-the-art of the available solutions with the purpose of fueling the research activities on this hot topic.

**Keywords:** MIMO radar; vital sign detection; heartbeat; breathing; human localization; angle of arrival; AoA; antenna array; biomedical; physiological

---

## 1. Introduction

In the past decades, wearable and contactless health monitoring sensors have attracted huge attention [1]. The formers are able to provide continuous monitoring capabilities in a large set of scenarios and show reliable performance in terms of vital sign detection and body parts motion estimation [2,3]. Nonetheless, current wearable health monitoring devices, e.g., respiratory belt, smart watches, pulse oximeters, may result in uncomfor experiences because of the intrinsic contact to the body. People could refuse to wear contact-based sensors, thus severely restricting their application field. Moreover, even though they allow to measure one or more physiological parameters, they are usually not able to simultaneously monitor more than one subject at a time.

Great efforts have been devoted to investigating the possibility of detecting physiological parameters without any contact. To this aim, the most employed detection methodologies exploit thermal imaging, optical systems and radar-based devices [4,5].

The thermal imaging extraction of vital signs is based on the detection of the infrared (IR) radiation emitted by a certain part of the human body. The analyzed part of the human body takes the physiological effect into account [6,7]. As an example, the heart activity is related to the temperature variation caused by the blood flow at certain superficial arteries, whereas the respiratory activity involves the temperature gradient caused by breathing out. However, they are largely affected by random body motion artifacts and furthermore the possible applications are limited by the high cost of the sensor.

Optical systems are based on cameras whose main tasks rely on the extraction of the cyclic chest motions due to cardiorespiratory activities or to the detection of skin color changes as a consequence of the physiological movements (photoplethysmography) [8,9]. However, they are very sensitive to different ambient light conditions and affected by privacy concerns that make these transducers unsuitable for a huge set of applications.

Radar-based systems exploit the Doppler effect, i.e., the signal reflected by a person is modulated by the chest motion as a consequence of the physiological activity or of the skin pulse due to arterial blood pressure. In this framework, the use of radar sensors for the non-contact detection of the Doppler effect has become a rapidly developing research field fueled by the great technological advancements, particularly concerning the microwave and millimeter-waves (mm-) front-ends [10–12]. Radar features outperform the other contactless methods, e.g., ultrasonic and infrared, in terms of reliability in presence of changing light conditions and temperature.

Medical radars typically exploit sensing techniques and technologies such as ultra-wideband (UWB), Doppler, continuous wave (CW), and frequency modulated continuous wave (FMCW) radars [13–20]. They can be considered as un-intrusive systems able to preserving the users' privacy and comfort.

Whereas CW radars provide better resolution than FMCW radars in measuring speeds and displacements, FMCW radars are able to provide range detection capabilities [21–23]. UWB radars are characterized by low transmitted power and power consumption [24].

In recent years, multiple-input multiple-output (MIMO) radars are achieving a growing attention because of their capability to measure the angle-of-arrival (AoA) of the received echoes thus enabling the estimation of the targets' precise location over both the azimuthal and the elevation planes. The peculiar hardware characteristic of the MIMO radar architectures is the presence of multiple transmitting and receiving antennas able of transmitting different, often orthogonal waveforms. Thereafter, by measuring the time shifts resulting from the different time-of-flight (TOF) covered by the echoes reflected by targets with different angular positions, it is possible to compute the AoAs and thus estimate the exact targets location [25].

The most relevant advantages of this technology can be summarized as:

- Improved detection performances due to the signal-to-noise (SN) ratio of the received signals better than the single-input-single-output systems.
- Angle estimation capabilities.
- Lower minimum detectable speed.

The available research articles concerning MIMO radars for biomedical applications are divided into two main topics:

1. MIMO systems exploited for enhancing the accuracy and reliability of the vital sign detection.
2. MIMO systems employed for both the human vital sign detection and human precise location.

In this contribution, an insight on the main feature of the MIMO technology and a review of the more recent developments along with the future challenges for biomedical applications are provided. The purpose of this work is to stimulate new ideas, concepts, and theories and to foster further applications addressed to the researchers in the field.

To the best of the authors' knowledge, the review papers currently available among the scientific records are specifically focused on the MIMO technology or on the vital sign detection separately, with no examples analyzing the topic of the biomedical MIMO radars for vital sign detection and human localization. The lack of papers collecting and illustrating the main results in the field, fueled the authors' effort to fill this gap by writing this work.

The paper is organized as follows. In Section 2, the most relevant aspects of the body physiology and MIMO theory and technology are depicted. In Section 3, the most relevant work in the field are analyzed and commented. Finally, discussions and conclusions are outlined in Sections 4 and 5, respectively.

## 2. Preliminary Background

### 2.1. Body Physiology

Two of the most investigated physiological parameters for the design of contactless sensors are the breathing and heart rates.

The main role of the respiratory system is the gas exchange from the inside out of the body and the vice versa. In detail, the body inhales the oxygen ( $O_2$ ) needed by the body cells and exhales the carbon dioxide ( $CO_2$ ) waste production. The  $O_2$  passes through the upper respiratory system, the trachea and the bronchi and reaches the lungs. The bronchi repeatedly fork until they form the alveoli inside the lungs. The alveoli themselves are responsible for the gas exchange with the blood, thereafter the  $CO_2$  travels the inverse path and it is exhaled. The effects of the respiratory system in terms of external chest movements are the combination of rib cage and abdominal motions, namely 9 to 24 breaths-per-minute, on average. Tough the amplitude of the chest displacement depends on the relative position between the observer and the chest itself, typical values range from 4 mm to 12 mm [26].

The blood pumped by the heart contractions is carried throughout the body circulatory system by means of the cardiovascular system. The circulatory system is composed of two main stages that are circularly and continuously traveled. First, the pulmonary circulation pushes the blood from the heart to the lungs for absorbing  $O_2$  and releasing  $CO_2$  and brings the full-of-oxygen blood back to the heart. Thereafter, the systemic circulation delivers the blood from the heart to the body and finally the blood devoid of  $O_2$  returns to the heart and the process is repeated again [27].

As in the case of the respiratory system, the heart pumping induces a motion of the skin surface. Although the extent of this motion depends on many physiological parameters, average peak-to-peak displacement values are between 0.4 mm and 0.6 mm, whereas the heart rate ranges from 50 to 90 beats-per-minutes, on average.

If an electromagnetic signal hits the human body, the chest motion  $x_{bh}$  due to both the breathing activity and heartbeat involves a phase shift  $\phi_{bh}$  on the reflected waveform that can be assessed as:

$$\phi_{bh} = x_{bh} \frac{4\pi f_c}{c} \quad (1)$$

where  $f_c$  is the central operating frequency and  $c$  is the speed of the light.

The measurement of  $\phi_{bh}$  is usually the purpose of the systems employed for the vital sign detection.

### 2.2. MIMO Theory

The MIMO concept involves the presence of multiple radiating and receiving sections [28]. The role of the radar is to process the data coming from the surrounding space by following different approaches that, according to modern paradigms, are model-based. The model-based approach relies on hypothesis concerning the data observed in the real world, with the purpose of creating an artificial model well-fitting the real scenarios of interest.

To this purpose, the following hypothesis have been assumed throughout the theoretical description [29]:

- Isotropic and linear transmission medium: this ensures that the propagation properties do not change with the AoA and that the received signals can be computed as a linear superposition of the signal wave fronts generated by the reflecting objects.
- Far-field assumption: this ensures that the received signals can be considered as parallel to each other. It is usually a reasonable assumption by ensuring the distance between the targets and the radar be much larger than the dimension of the antenna array. A rule of thumb for verifying this assumption is provided in [30], i.e., the distance radar-target is larger than  $2D^2/\lambda$ , with  $D$  being the dimension of the antenna array and  $\lambda$  the wavelength of the signals.

- Narrowband assumption: this ensures that the frequency components of the received signals are grouped around the carrier frequency. Therefore, by considering  $n$  reflecting objects generating  $n$  source signals  $s_n^r(t)$  ( $n = [1, 2, \dots, N]$ ):

$$s_n^r(t) = \alpha_n(t) \cos(2\pi f_c t + \beta_n(t)) \quad (2)$$

where,  $\alpha_n(t)$  and  $\beta_n(t)$  are the signals amplitudes and phases, respectively.

- Additive White Gaussian Noise (AWGN) channel: the noise content is uncorrelated.

The main features of the MIMO techniques exploit the AoA detection capabilities that are in turn based on the measurement of phase differences. Let us consider an object generating an electromagnetic wave directed toward and detected by a two-element antenna array, separated by a distance  $d$ .

It can be considered that the received waves impinge on the antennas at an angle  $\theta$ , therefore, by supposing that the object is closer to the first element, the wave path from the object to the second element is longer by an additional distance  $\Delta = d \cdot \sin \theta$ . By considering the signal received by the first antenna as a reference, namely  $x_1(t) = s(t)$ , the signal received by the second element  $x_2(t)$  is:

$$x_2(t) = s(t) e^{-j \frac{2\pi}{\lambda} d \cdot \sin \theta} \quad (3)$$

This scenario is graphically reproduced in Figure 1.

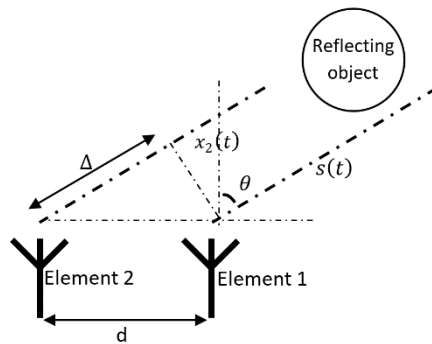


**Figure 1.** Configuration with a two-element receiving array.

In a similar fashion, by considering  $m$  receiving antennas ( $m = [1, 2, \dots, M]$ ), the received signals  $x_m(t)$  at the  $m$ th antenna can be expressed in matrix form as follow:

$$\begin{bmatrix} x_1(t) \\ x_2(t) \\ \vdots \\ x_M(t) \end{bmatrix} = \begin{bmatrix} a(\theta_1) \\ a(\theta_2) \\ \vdots \\ a(\theta_N) \end{bmatrix} \cdot s(t) + \begin{bmatrix} n_1(t) \\ n_2(t) \\ \vdots \\ n_m(t) \end{bmatrix} \quad (4)$$

where  $a(\theta) = [1 \quad e^{j \frac{2\pi}{\lambda} d \cdot \sin \theta} \quad \dots \quad e^{j \frac{2\pi}{\lambda} d \cdot \sin \theta_{n-1}}]^T$  is the steering vector and  $n_m(t)$  denotes the interferences plus-noise term.

According to the previous considerations, the key step of the AoA detection involves the measurement of the phase shift  $\frac{2\pi}{\lambda} d \cdot \sin \theta_n$ . Thereafter, the corresponding angle of arrival can be computed by:

$$\theta = \sin^{-1} \left( \frac{\Delta \cdot \lambda}{2\pi d} \right) \quad (5)$$

In real scenarios, determining the AoA based only on phase differences might not be a reliable solution, particularly in case of multiple incoming signals. To this aim, in the scientific literature, different algorithms are proposed. The most popular techniques can be classified into conventional beamforming techniques, subspace-based techniques, and maximum likelihood (ML) techniques [29].

Beamforming techniques are based on “steering” the antenna array in the direction of the AoA in order to notice the maximum power [30]. After selecting the desired direction, a weight vector can be employed to combine the available data in a single signal. Examples of beamforming techniques are the conventional beamformer, the Capon’s beamformer, the minimum variance distortion-less response (MVDR), the linear prediction, and the Bartlett method [31–34]. Although they offer better performance, particularly in case of low signal-to-noise ratio, ML techniques are less employed because of their high computational cost [35]. They consist in reconstructing the signal waveform with only the components of the desired AoA. In subspace-based techniques, the data space is partitioned into two orthogonal subspaces, i.e., the signal and noise subspaces. The former corresponds to the steering vectors and it is associated to the larger eigenvalues of the correlation matrix, the latter is spanned by the smaller eigenvalues. Some popular examples are multiple signal classification (MUSIC) algorithm, minimum norm method, and estimation of signal parameters via rotational invariance techniques (ESPRIT) [36–39].

A key aspect of the MIMO detection capabilities concerns the antennas arrangement. Two popular antenna configurations are the uniform linear array (ULA) and uniform rectangular array (URA) [29]. ULA consists of  $M$  antenna elements aligned and equally spaced on a straight line. A possible configuration is shown in Figure 2.

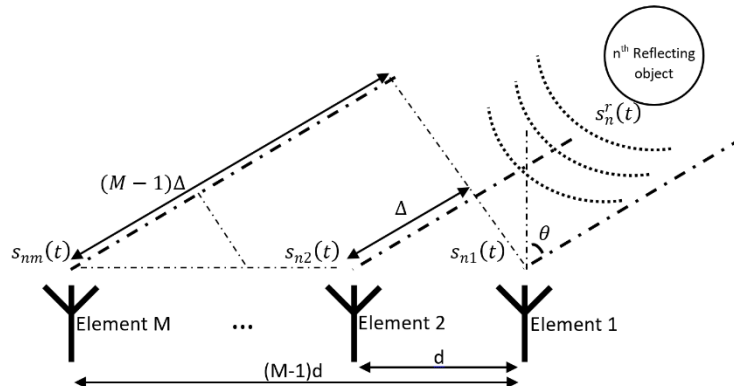


**Figure 2.** Uniform linear array (ULA) configuration.

In this case,  $s_n^r(t)$  impinges on the antennas after a delay  $\tau_d$  proportional to the target range  $R$ , according to  $\tau_d = \frac{R}{c}$ . Therefore, the signal received by the first element  $s_{n1}(t)$  is a time-shifted version of  $s_n^r(t)$ :

$$s_{n1}(t) = \alpha_n(t - \tau_d) e^{-j[2\pi f_c(t - \tau_d) + \beta_n(t - \tau_d)]} \quad (6)$$

According to (3), the signal at the  $m$ th element is a delayed version of the signal received by the first element, in detail:

$$s_{nm}(t) = \alpha_n(t - \tau_d) e^{-j[2\pi f_c(t - \tau_d) + \beta_n(t)]} e^{j(m-1)\frac{2\pi}{\lambda}d \sin \theta_n} \quad (7)$$

The additional factor in (7)  $e^{j(m-1)\frac{2\pi}{\lambda}d \sin \theta_n}$  depends on the element position relative to the first one and on the product  $d \cdot \sin \theta_n$ . With the aim of extracting the  $\theta_n$ , the phase shifts must be limited to the interval  $[-\pi, \pi]$  and in turn the possible AoA to  $[-90^\circ, 90^\circ]$ . This requires an antenna element spacing less than  $\frac{\lambda}{2}$  otherwise there will be an ambiguity in the angle estimation.

$$x_m(t) = s_n(t) \sum_{n=1}^N e^{-j\frac{2\pi}{\lambda}d \cdot \sin \theta_n(m-1)} + n_m(t) \quad (8)$$

Equation (7) is often reported in matrix form as follow:

$$x(t) = \begin{bmatrix} a(\theta_1) & a(\theta_2) & \dots & a(\theta_N) \end{bmatrix} \begin{bmatrix} s_1(t) \\ s_2(t) \\ \vdots \\ s_M(t) \end{bmatrix} + \begin{bmatrix} n_1(t) \\ n_2(t) \\ \vdots \\ n_m(t) \end{bmatrix} \quad (9)$$

On the other hand, URA is a kind of two-dimensional array enabling both azimuth and elevation estimation. Three different typical centro-symmetric two-dimensional array configurations with different elements positioning are shown in Figure 3.

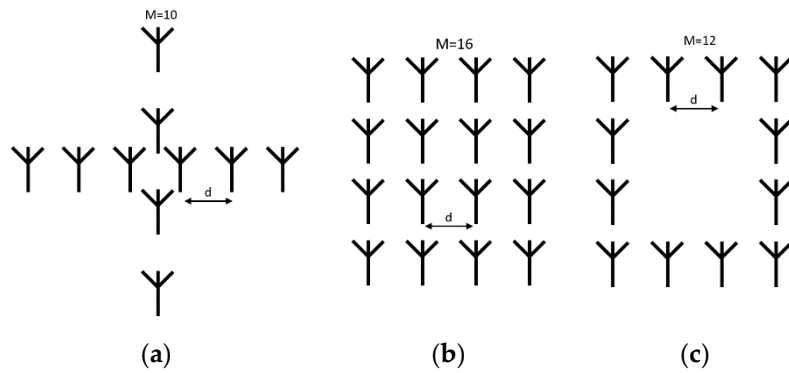


**Figure 3.** (a–c) Typical uniform rectangular array (URA) configurations.

Compared to the steering matrix and consequently the AoA processing of ULA, the case of URA is different because it takes into account both the azimuth and elevation angles.

It is clear that the greater the number of antennas, the better the radar performance. As an example, for the case of  $M$  equally spaced antennas separated by a distance of  $\frac{\lambda}{2}$ , the angle resolution is equal to  $\frac{\lambda}{M}$ . As a matter of fact, MIMO radar is synonym of superior performance because it allows to get additional RX antennas, i.e., virtual antennas, without increasing the hardware complexity of the receiver chain in terms of added low-noise amplifiers, mixers, filters, and analog-to-digital converters. Indeed, the number of antennas of a MIMO radar corresponds to a single-input-single-output (SIMO) radar with one transmitter and  $N \times M$  receivers, thus providing a cost-effective way to enhance the angle resolution capabilities. An example of 2Tx4R MIMO radar array has been reported in Figure 4.

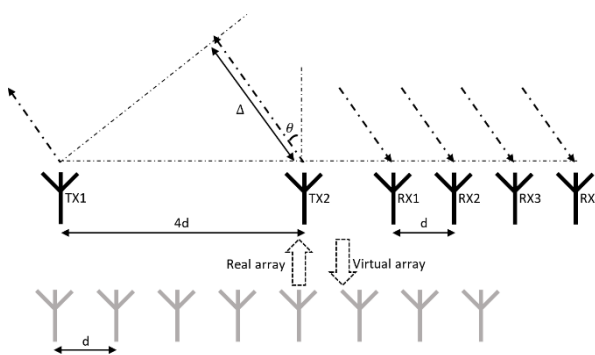


**Figure 4.** 2Tx4R multiple-input-multiple-output (MIMO) radar array.

The signal emitted by the two transmitting antennas will result in a steering vector equal to  $[1 \ e^{j\pi \cdot \sin \theta_n} \ e^{j2\pi \cdot \sin \theta_n} \ e^{j3\pi \cdot \sin \theta_n} \ e^{j4\pi \cdot \sin \theta_n} \ e^{j5\pi \cdot \sin \theta_n} \ e^{j6\pi \cdot \sin \theta_n} \ e^{j7\pi \cdot \sin \theta_n}]$ , synthesizing a virtual array of eight elements. Two popular approaches employed for separating the signals coming from the two different transmitters involve the orthogonality between the transmitting channels and

they exploit time division multiplexing (TDM) or binary phase modulation (BPM) [25]. In the former, the transmission is divided in time slots attributed to each different transmitting antenna, whereas in the latter the transmission between the two channels is simultaneous while the phases are 0 or  $\pi$ .

By way of explanation, a typical architecture of a 2Tx4R MIMO radar has been reproduced in Figure 5. For each transmitting channel, a digital processing unit generates the initial signal that is successively up-converted by a frequency multiplication stage, amplified and transmitted by a high-power amplifier (HPA) and the corresponding antenna element, respectively. The received signal is amplified by a low-noise amplifier, down-converted and finally processed by the digital processing unit.

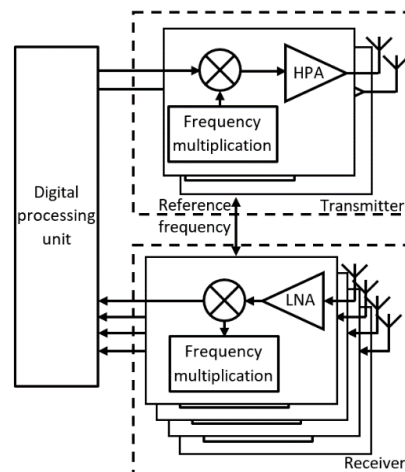


**Figure 5.** Typical 2Tx4R MIMO radar architecture.

### 3. Biomedical Application of MIMO Radars

In [40–42] some examples where a MIMO radar is exploited for the human detection in cluttered environments are shown. In detail, in [42] a bistatic MIMO radar has been employed for estimating the target location. The conceptual scheme of the system presented in this work is shown in Figure 6.

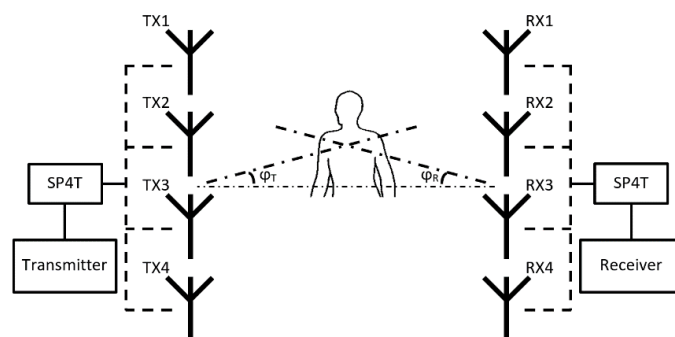


**Figure 6.** Conceptual scheme of the bistatic radar reported in [42].

In the proposed configuration, operating at 2.4 GHz, the transmitter and the receiver have been set opposite each other, 4 m apart. The position of the person has been detected by intersecting the lines lying on the angles  $\varphi_T$  and  $\varphi_R$ , i.e., the AoA at the transmitting and receiving sections, respectively. Since the humans' echoes fluctuate due to the physiological activity, the undesired echoes from stationary objects can be recognized and discarded. The effectiveness of the proposed solution has been confirmed in multipath environments with the subject-under-test in different positions.

In [43], a radar working within the Ka band exploits an antenna array composed by 256 equidistant virtual elements for both people localization and breathing detection. The measured data have been organized in beamformed images and thereafter transformed from the slow-time to the Doppler

domain in order to isolate the static objects in the scene. Unlike [42], in [43] stationary people have been considered static objects, thus ignoring the motion related to the physiological activity. Different scenarios including up to three people have been considered. Moreover, various windows have been applied on the measured data for improving the detection. Although limited to the detection of static objects, this radar showed valuable performance for the simultaneous monitoring of multiple targets in large areas.

In [44], a feasibility study concerning the extraction of the radar image of the human heart by using an UWB radar has been proposed. The UWB radar is composed by a vector network analyzer (VNA), a switching system, a beamformer and the antennas. In detail, a 56-elements non-uniform antenna array has been placed in contact with the thorax of a 35 years-old subject, while the breathing rate has been measured by means of an electrocardiogram (ECG). The VNA and the ECG measurements are synchronized by means of a trigger signal, whereas the operating frequency spans from 0.75 GHz to 12.27 GHz. The collected data are exploited for the task of image extraction by implementing a delay and sum (DAS)-based beamformer. A schematic diagram of the system has been reported in Figure 7.

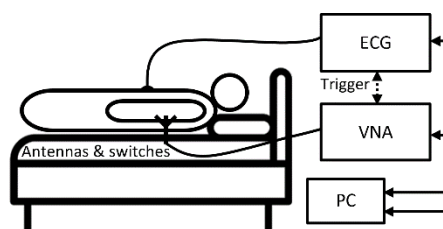


**Figure 7.** Schematic diagram of the ultra-wideband (UWB) radar proposed in [44].

Since a precise knowledge of the body inner structure was not available, a clear evidence of the presented results was not clearly stated throughout [44]. However, the detected points were in agreement with the expected location of the heart sections and the measured breathing rate corresponded to the ECG measurement.

The work reported in [45], demonstrated the concurrent breathing and heartbeat measurement capabilities by using a MIMO radar that exploits a TDM technique. Four transmitting/receiving couples of antennas have been randomly distributed around a person standing 4 m away from the radar. A graphical representation of the scenario has been shown in Figure 8.

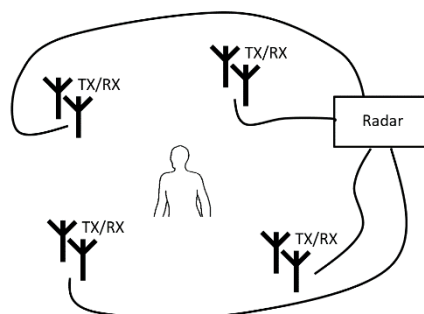


**Figure 8.** Graphical representation of the operating scenario described in [45].

The 16 collected acquisitions allowed both to increase the SN of the received signal and to enhance the reliability of the measurement. Indeed, the signal received by a single transmitting/receiving couple might be vanishing or weak due to different factors, e.g., multipath from cluttered environments and/or excessive angulations. The redundant detection from multiple angles allows to overcome these limitations, thus fulfilling the task of measuring both the breathing rate and the heartbeat.

In [46], both the angular position and the breathing of two people located at different lateral positions but at the same distance has been demonstrated. The proposed system employs an UWB radar

and implements an adaptive beamforming technique, i.e., a modified Capon method with optimized weights at each receiving antenna. The optimization was implemented because the Capon method requires not correlated received signals, as it is not the case of the echoes reflected from breathing people. In detail, two diagonal loading factors have been tested for the AoA estimation, exhibiting a root-mean-square error of the measured breathing better than 0.13 mm, which is a remarkable result compared to the performance of the conventional algorithm that has been estimated equal to 2.7 mm.

Reference [47] reports on a human localization algorithm implementing a 2-D MUSIC algorithm with spherical-mode applied on a time-differential channel. By means of a MIMO radar architecture, it has been demonstrated that the feasibility of both heartbeat and breathing detection in just few seconds, corresponding to one biological activity cycle. The experimental activity in indoor environment showed a localization error better than 0.5 m.

In [48], an FMCW MIMO radar has been employed for monitoring both the breathing and heart rates. The proposed system, after noise suppression and unwanted targets removal, improves the standard accuracy levels by exploiting multiple antenna pairs operating simultaneously.

In [49], the person 3D location is estimated by employing a time-differential channel technique whereas the Doppler radar cross section (RCS) is calculated from the reflected signal. The received data are elaborated by exploiting a three-dimensional MUSIC algorithm with a spherical mode vector, whereas the person posture is identified by implementing a nearest neighbor algorithm.

The results showed that all postures had root-square mean error values within 0.25 m.

A graphical representation of the measurement setup and the experimental environment is provided in Figure 9. The antenna arrays have been realized on a polytetrafluoroethylene (PTFE) substrate and are composed by 16 patches per channel, i.e., transmitting and receiving channels.

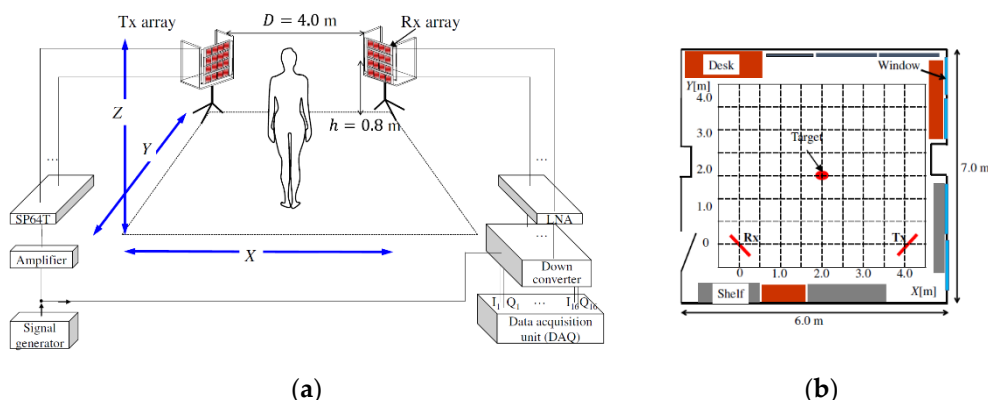


**Figure 9.** (a) Measurement setup and (b) experimental environment [49].

Not-human targets are discarded by observing the time-variant channel response of Figure 10, where humans show a time-varying behavior.

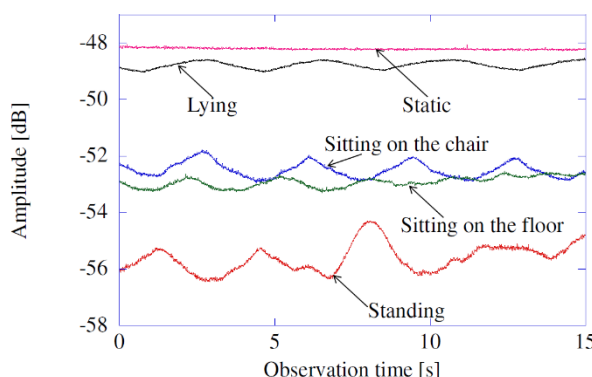


**Figure 10.** Response of time-variant channel [49].

As shown in Figure 11, where the measurements have been performed on a single person (a,b) standing, (c,d) sitting on a chair, and (e,f) lying on the floor, the different postures might be clearly recognized with good accuracy.

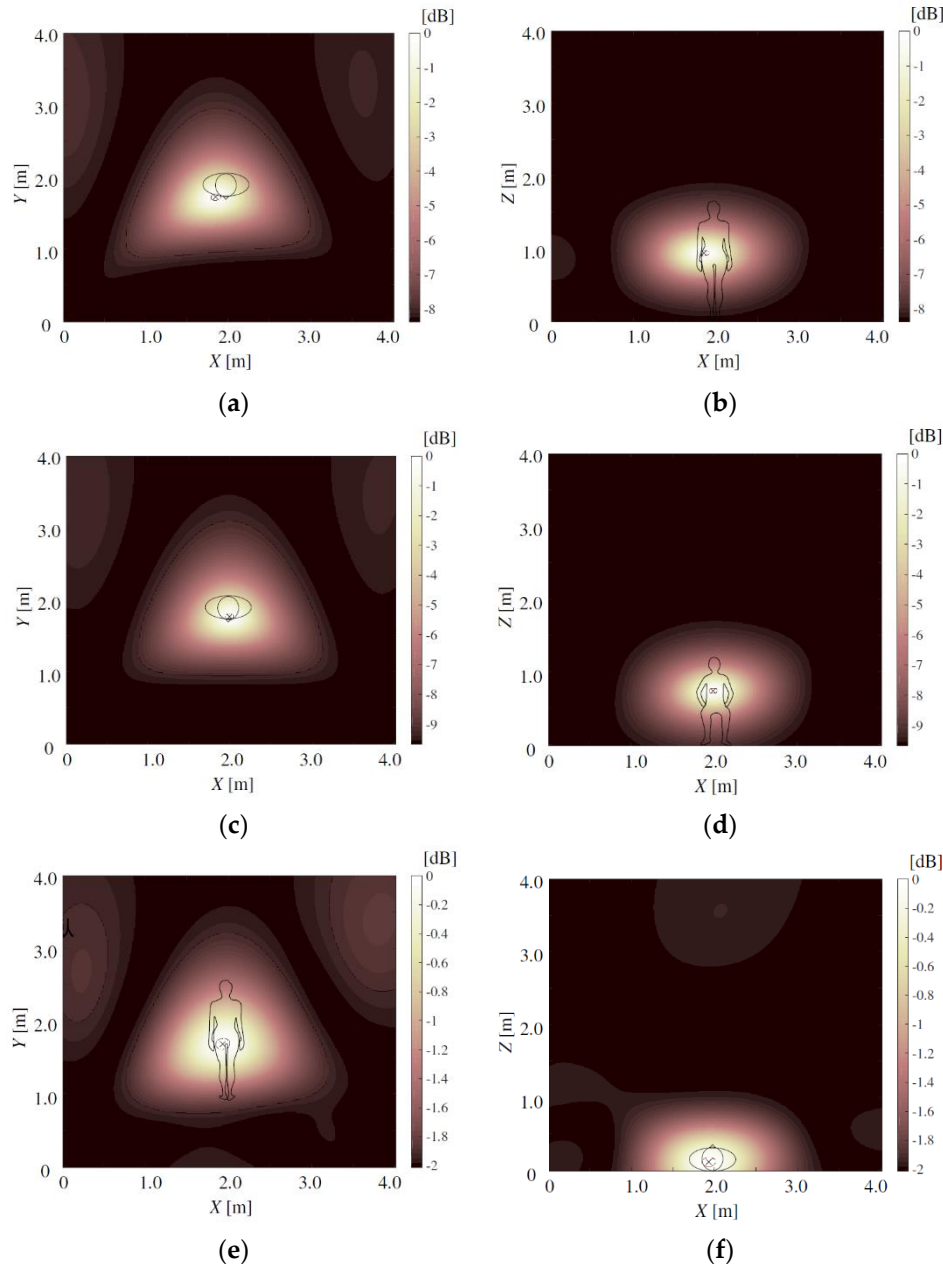


**Figure 11.** Multiple signal classification (MUSIC) spectrum with a person (a,b) standing, sitting on a chair (c,d), and (e,f) lying on the floor [49].

Moreover, the training data achieved from the height and the Doppler radar cross section (RCS) and reported on the scatter diagram of Figure 12, demonstrated that the postures do not have overlapping distributions.

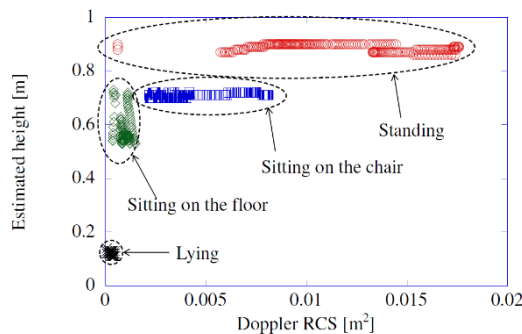


**Figure 12.** Training data based on height and Doppler radar cross section (RCS) [49].

A further example of radar application where multiple receiving antennas are employed for improving the detection capabilities in a redundant arrangement has been reported in [50]. In detail, a SIMO Doppler radar sensor has been developed in order to be sensitive only to moving objects. The additional receiving channel allowed to obtain the initial target location, whereas a subcarrier modulation has been implemented to solve the phase ambiguity issues. Finally, the exact position of only the moving object has been obtained.

In [51], the vital signs detection of multiple people employing a CW Doppler radar based on concurrent multibeam systems has been demonstrated. The multi-beam architecture allows to overcome the phase collision issues arising when multiple targets are present within the scene. Moreover, additional spatial filtering mitigates the inter-beam inferences.

In [52], the task of simultaneously detecting the people position and both the breathing and heart rates has been fulfilled by employing a very compact radar solution. A high integration level has been achieved by employing an operating frequency equal to 120 GHz. The antennas consist of two transmitters and eight receivers arranged in a circular distributed virtual array shape. Because of the circular distribution, a back-projection processing is required for the 3D image estimation.

In [53], the heartbeat rate of a person has been recorded during the sleeping time by using an UWB MIMO radar. In detail, the MIMO features have been exploited to improve the SN ratio by implementing a maximum ratio combining (MRC) technique. The MRC has been also used for avoiding the interferences due to the human unconscious movements during the sleep time.

A beamforming technique has been implemented at the radar receiver of the SIMO system presented in [54] for enhancing the desired signals and attenuating the unwanted components from other directions.

In [55], a MIMO radar system has been simulated with the purpose of locating the position of the patient and measuring the breathing rate. A custom antenna array has been also designed and tested.

#### 4. Discussion

To the best knowledge of the authors, the works reported in Section 4 are among the most relevant concerning the MIMO radar technology employed for the vital sign detection. Even though within the scientific literature different works separately addressed the tasks of vital sign detection and multiple target location, only few contributions are directed to the concomitant investigation of these two tasks. The main properties of the reported papers have been summarized in Table 1.

Different purposes have been fulfilled within the research activities of Section 4. In detail, refs. [42,43,45,46,48,51–55] employs the presence of multiple antennas for increasing the SN at the receiver, in turn improving the accuracy and the reliability of the vital sign detection. The enhanced performance are the result of the increased transmitted power through multiple transmitters and of the different AoA of the received signals that allow to avoid vanishing or weak echoes. In [42,43,46,47,49,50,52,55], the features of MIMO radars have been used for adding the human precise localization capability to the vital sign detection. An unconventional application has been reported in [44] addressing the task of creating a radar image of the human heart. Although the paper has

been published in year 2014 and the research topic has not been continued, the challenge of creating a radar-based image of the heart is still actual and noteworthy.

Different frequencies ranging from 0.75 GHz to 120 GHz have been employed whereby the increased hardware and processing complexity of higher frequency radars is well awarded by the premium performance in terms of system integration, spatial resolution and accuracy. An unresolved challenge appears to be the capability to estimate the vital signs in presence of random body movements or radar platform motion. These serious issues are very common in a huge range of applications and occur when the target or the radar platform cannot be maintained stationary, respectively. Indeed, these additional movements might mask the tiny phase shift due to vital signs thus making its detection unfeasible.

Moreover, the investigation of intrabeam interferences and spectrum leakages seems not to be adequately addressed. In detail, the existence of undesired noise at different range bins could involve ghost targets detection or degrade the signals of interest.

Different papers face the issue of the multiple target detection only in stationary environments thus reducing the complexity of the analyzed scenario not accounting for range migration effects.

**Table 1.** Main properties of the reported biomedical MIMO radars.

Ref. n.	Radar Configuration	Measured Parameters	Number of Targets	Signal Processing	MIMO Configuration	Operating Frequency
[42]	Bistatic	Human localization	Single human target	MUSIC algorithm	4Tx4R	2.47 GHz
[43]	Monostatic	Human localization, breathing detection	Multiple human targets	Frequency analysis	16Tx16R	36.44 GHz
[44]	Monostatic	Heart imaging	Single human target	DAS beamformer	7x8T/R	0.75 GHz–12.27 GHz
[45]	Bistatic	Breathing detection	Single human target	Frequency analysis	4Tx4R	94 GHz
[46]	Monostatic	Human localization, breathing detection	Multiple human targets	Modified Capon beamformer	1Tx4R	60.5 GHz
[47]	Monostatic	Human localization	Multiple human targets	MUSIC algorithm	4Tx4R & 8Tx8R	2.47 GHz
[48]	Monostatic	Heart and breathing detection	Single human target	Frequency analysis	1Tx4R	3.3 GHz–10.3 GHz
[49]	Bistatic	Human localization, posture identification	Single human target	MUSIC algorithm	16Tx16R	2.47 GHz
[50]	Monostatic	Human and moving objects localization	Single target	Cooperative tracking-algorithm	1Tx3R	5.8 GHz
[51]	Monostatic	Heart and breathing detection	Multiple human targets	Concurrent multibeam	4Tx4R	2.4 GHz
[52]	Monostatic	Human localization, breathing and heartbeat detection	Multiple human targets	Frequency analysis	2Tx8R	120 GHz
[53]	Monostatic	Heartbeat detection	Single target	Maximum ratio combining	2Tx4R	60.5 GHz
[54]	Monostatic	Breathing detection	Single target	Beamforming	1Tx8R	5.8 GHz
[55]	Monostatic	Human localization, heartbeat detection	Single target	Frequency analysis	1Tx4R	5.8 GHz

## 5. Conclusions

In this review article, an extensive survey on the MIMO technology and its applications on the vital sign detection and human localization have been reported.

The main features of MIMO radars have been exposed for highlighting the main advantages over the traditional single-input-single-output architectures with the aim of fueling the research activity on this interesting and recent topic. After a description of the involved physiological mechanisms and a straightforward theoretical analysis of the MIMO processing techniques, the main findings concerning the MIMO radar technology for the vital sign detection and human localization have been reported. The aim of this work is to provide a landmark for the future research activities in the context of biomedical radars.

**Author Contributions:** Conceptualization, formal analysis, methodology, investigation, original draft preparation E.C.; review and editing, supervision, funding acquisition, A.C. All authors have read and agreed to the published version of the manuscript.

**Funding:** This research received no external funding.

**Conflicts of Interest:** The authors declare no conflict of interest.

## References

1. Dinh, T.; Nguyen, T.; Phan, H.-P.; Nguyen, N.-T.; Dao, D.V.; Bell, J. Stretchable respiration sensors: Advanced designs and multifunctional platforms for wearable physiological monitoring. *Biosens. Bioelectron.* **2020**, *166*, 112460. [[CrossRef](#)]
2. Lo Presti, D.; Carnevale, A.; D’Abbraccio, J.; Massari, L.; Massaroni, C.; Sabbadini, R.; Zaltieri, M.; Di Tocco, J.; Bravi, M.; Miccinilli, S.; et al. A multi-parametric wearable system to monitor neck movements and respiratory frequency of computer workers. *Sensors* **2020**, *20*, 536. [[CrossRef](#)] [[PubMed](#)]
3. Massaroni, C.; Di Tocco, J.; Bravi, M.; Carnevale, A.; Presti, D.L.; Sabbadini, R.; Miccinilli, S.; Sterzi, S.; Formica, D.; Schena, E. Respiratory monitoring during physical activities with a multi-sensor smart garment and related algorithms. *IEEE Sens. J.* **2020**, *20*, 2173–2180. [[CrossRef](#)]
4. Cardillo, E.; Di Mattia, V.; Manfredi, G.; Russo, P.; De Leo, A.; Caddeemi, A.; Cerri, G. An electromagnetic sensor prototype to assist visually impaired and blind people in autonomous walking. *IEEE Sens. J.* **2018**, *18*, 2568–2576. [[CrossRef](#)]
5. Khanam, F.-T.-Z.; Al-Naji, A.; Chahl, J. Remote monitoring of vital signs in diverse non-clinical and Clinical scenarios using computer vision systems: A review. *Appl. Sci.* **2019**, *9*, 4474. [[CrossRef](#)]
6. Bennett, S.; El Harake, T.N.; Goubran, R.; Knoefel, F. Adaptive eulerian video processing of thermal video: An experimental analysis. *IEEE Trans. Instrum. Meas.* **2017**, *66*, 2516–2524. [[CrossRef](#)]
7. Garbey, M.; Sun, N.; Merla, A.; Pavlidis, I. Contact-free measurement of cardiac pulse based on the analysis of thermal imagery. *IEEE Trans. Biomed. Eng.* **2007**, *54*, 1418–1426. [[CrossRef](#)]
8. Poh, M.-Z.; McDuff, D.J.; Picard, R.W. Advancements in noncontact, multiparameter physiological measurements using a webcam. *IEEE Trans. Biomed. Eng.* **2011**, *58*, 7–11. [[CrossRef](#)]
9. Sun, Y.; Thakor, N. Photoplethysmography revisited: From contact to noncontact, from point to imaging. *IEEE Trans. Biomed. Eng.* **2016**, *63*, 463–477. [[CrossRef](#)]
10. Caddeemi, A.; Cardillo, E. Optical control of gain amplifiers at microwave frequencies. In Proceedings of the Computing and Electromagnetics International Workshop, Barcelona, Spain, 21–24 June 2017; pp. 51–52. [[CrossRef](#)]
11. Visweswaran, A. 9.4 a 145 GHz FMCW-radar transceiver in 28nm CMOS. In Proceedings of the IEEE International Solid-State Circuits Conference, San Francisco, CA, USA, 17–21 February 2019; pp. 168–170. [[CrossRef](#)]
12. Caddeemi, A.; Cardillo, E.; Crupi, G. Light activation of noise at microwave frequencies: A study on scaled gallium arsenide HEMT’s. *IET Circ. Device. Syst.* **2018**, *12*, 242–248. [[CrossRef](#)]
13. Ren, L.; Wang, H.; Naishadham, K.; Kilic, O.; Fathy, A.E. Phase based methods for heart rate detection using UWB impulse Doppler radar. *IEEE Trans. Microw. Theory Tech.* **2016**, *64*, 3319–3331. [[CrossRef](#)]
14. Cardillo, E.; Li, C.; Caddeemi, A. Empowering blind people mobility: A millimeter-wave radar cane. In Proceedings of the IEEE International Workshop on Metrology for Industry 4.0 & IoT, Roma, Italy, 3–5 June 2020; pp. 213–217. [[CrossRef](#)]
15. Rittiplang, A.; Phasukkit, P.; Orankitanun, T. Optimal central frequency for non-contact vital sign detection using monocycle UWB radar. *Sensors* **2020**, *20*, 2916. [[CrossRef](#)] [[PubMed](#)]
16. Wang, Y.; Wang, W.; Zhou, M.; Ren, A.; Tian, Z. Remote monitoring of human vital signs based on 77-GHz mm-wave FMCW radar. *Sensors* **2020**, *20*, 2999. [[CrossRef](#)]
17. Cardillo, E.; Caddeemi, A. Feasibility study to preserve the health of an industry 4.0 worker: A radar system for monitoring the sitting-time. In Proceedings of the IEEE Workshop on Metrology for Industry 4.0 and IoT, Naples, Italy, 4–6 June 2019; pp. 254–258. [[CrossRef](#)]
18. Cardillo, E.; Caddeemi, A. Insight on electronic travel aids for visually impaired people: A review on the electromagnetic technology. *Electronics* **2019**, *8*, 1281. [[CrossRef](#)]
19. Yang, Z.-K.; Shi, H.; Zhao, S.; Huang, X.-D. Vital sign detection during large-scale and fast body Movements based on an adaptive noise cancellation algorithm using a single Doppler radar sensor. *Sensors* **2020**, *20*, 4183. [[CrossRef](#)]
20. Caddeemi, A.; Cardillo, E. Automotive anti-abandon systems: A millimeter-wave radar sensor for the detection of child presence. In Proceedings of the IEEE International Conference on Advanced Technologies, Systems and Services in Telecommunications, Nis, Serbia, 23–25 October 2019; pp. 94–97. [[CrossRef](#)]

21. Rodriguez, D.; Li, C. Sensitivity and distortion analysis of a 125-GHz interferometry radar for submicrometer motion sensing applications. *IEEE Trans. Microw. Theory Tech.* **2019**, *67*, 5384–5395. [[CrossRef](#)]
22. Kim, S.; Nguyen, C. A displacement measurement technique using millimeter-wave interferometry. *IEEE Trans. Microw. Theory Tech.* **2003**, *51*, 1724–1728. [[CrossRef](#)]
23. Cardillo, E.; Cademi, A. A novel approach for crosstalk minimization in FMCW radars. *Electron. Lett.* **2017**, *53*, 1379–1381. [[CrossRef](#)]
24. Immoreev, I.I.; Fedotov, P.G.S.D.V. Ultra wideband radar systems: Advantages and disadvantages. In Proceedings of the IEEE Conference on Ultra Wideband Systems and Technologies, Baltimore, MD, USA, 21–23 May 2002; pp. 201–205. [[CrossRef](#)]
25. Li, J.; Stoica, P. *MIMO Radar Signal Processing*, 1st ed.; Wiley: New York, NY, USA, 2009.
26. Hintermuller, C. *Advanced Biosignal Processing and Diagnostic Methods*, 1st ed.; InTechOpen: London, UK, 2016.
27. Al-Naji, A.; Gibson, K.; Lee, S.; Chahl, J. Monitoring of cardiorespiratory signal: Principles of remote measurements and review of methods. *IEEE Access* **2017**, *5*, 15776–15790. [[CrossRef](#)]
28. Bliss, D.W.; Forsythe, K.W. Multiple-input multiple-output (MIMO) radar and imaging: Degrees of freedom and resolution. In Proceedings of the 37th Asilomar Conf. Signals, Systems & Computers, Pacific Grove, CA, USA, 9–12 November 2003; Volume 1, pp. 54–59. [[CrossRef](#)]
29. Zhizang, C.; Gopal, K.G.; Yiqiang, Y. *Introduction to Direction-of-Arrival Estimation*, 1st ed.; Artech House: London, UK, 2010.
30. Balanis, C.A. *Antenna Theory: Analysis and Design*, 3rd ed.; Wiley: New York, NY, USA, 2005.
31. Krim, H.; Viberg, M. Two decades of array signal processing research. *IEEE Signal Proc. Mag.* **1996**, *13*, 67–94. [[CrossRef](#)]
32. Litva, J.; Lo, T.K.Y. *Digital Beamforming in Wireless Communications*; Artech House: Norwood, MA, USA, 1996.
33. Capon, J. High-resolution frequency-wavenumber spectrum analysis. *Proc. IEEE* **1969**, *57*, 2408–2418. [[CrossRef](#)]
34. Makhoul, J. Linear prediction: A tutorial review. *Proc. IEEE* **1975**, *63*, 561–580. [[CrossRef](#)]
35. Ziskind, I.; Wax, M. Maximum likelihood localization of multiple sources by alternating projection. *IEEE Trans. Acoust. Speech Signal Process.* **1998**, *36*, 1553–1560. [[CrossRef](#)]
36. Vander Veen, A.J.; Deprettere, E.F.; Swindlehurst, A.L. Subspace based signal analysis using singular value decomposition. *Proc. IEEE* **1993**, *81*, 1277–1308. [[CrossRef](#)]
37. Schmidt, R.O. Multiple emitter location and signal parameter estimation. *IEEE Trans. Antennas Propag.* **1986**, *34*, 276–280. [[CrossRef](#)]
38. HaHaardt, M.; Zoltowski, M.D.; Mathews, C.P.; Nossek, J. 2D unitary ESPRIT for efficient 2D parameter estimation. In Proceedings of the IEEE International Conference on Acoustics, Speech, and Signal Processing, Detroit, MI, USA, 9–12 May 1995; pp. 2096–2099. [[CrossRef](#)]
39. Roy, R.; Kailath, T. ESPRIT-estimation of signal parameters via rotational invariance techniques. *IEEE Trans. Acoust. Speech Signal Process.* **1989**, *37*, 984–995. [[CrossRef](#)]
40. Nango, M.; Honma, N.; Nishimori, K.; Sato, H. Biological activity detection method using MIMO system. *IEICE Commun. Express* **2013**, *2*, 36–41. [[CrossRef](#)]
41. Sasakawa, D.; Konno, K.; Honma, N.; Nishimori, K.; Takemura, N.; Mitsui, T.; Tsunekawa, Y. Localizing living body using bistatic MIMO radar in multi-path environment. In Proceedings of the European Conference on Antennas and Propagation, The Hague, The Netherlands, 6–11 April 2014; pp. 3253–3257. [[CrossRef](#)]
42. Konno, K.; Honma, N.; Sasakawa, D.; Tsunekawa, Y.; Nishimori, K.; Takemura, N.; Mitsui, T. Localizing multiple target using bistatic MIMO radar in multi-path environment. In Proceedings of the IEEE International Workshop on Electromagnetics, Sapporo, Japan, 4–6 August 2014; pp. 90–91. [[CrossRef](#)]
43. Biallawons, O.; Klare, J. Person localization by detection of breathing with the MIMO radar MIRA-CLE Ka. In Proceedings of the 10th European Conference on Synthetic Aperture Radar, Berlin, Germany, 3–5 June 2014; pp. 1–4.
44. Brovoll, S.; Berger, T.; Paichard, Y.; Aardal, Ø.; Lande, T.S.; Hamran, S. Time-lapse imaging of human heart motion with switched array UWB radar. *IEEE Trans. Biomed. Circuits Syst.* **2014**, *8*, 704–715. [[CrossRef](#)]
45. Walterscheid, I.; Smith, G.E. Respiration and heartbeat monitoring using a distributed pulsed MIMO radar. In Proceedings of the 39th Annual International Conference of the IEEE Engineering in Medicine and Biology Society, Seogwipo, Korea, 11–15 July 2017; pp. 3449–3452. [[CrossRef](#)]

46. Muragaki, M.; Okumura, S.; Maehara, K.; Sakamoto, T.; Yoshioka, M.; Inoue, K.; Fukuda, T.; Sakai, H.; Sato, T. Noncontact respiration monitoring of multiple closely positioned patients using ultra-wideband array radar with adaptive beamforming technique. In Proceedings of the IEEE International Conference on Acoustics, Speech and Signal Processing, New Orleans, LA, USA, 5–9 March 2017; pp. 1118–1122. [[CrossRef](#)]
47. Sasakawa, D.; Honma, N.; Nakayama, T.; Iizuka, S. Fast living-body localization algorithm for MIMO radar in multipath environment. *IEEE Trans. Antennas Propag.* **2018**, *66*, 7273–7281. [[CrossRef](#)]
48. Liu, Q.; Guo, H.; Xu, J.; Wang, H.; Kageza, A.; AlQarni, S.; Wu, S. Non-contact non-invasive heart and respiration rates monitoring with MIMO radar sensing. In Proceedings of the IEEE Global Communications Conference, Abu Dhabi, UAE, 9–13 December 2018; pp. 1–6. [[CrossRef](#)]
49. Sasakawa, D.; Honma, N.; Nakayama, T.; Iizuka, S. Human posture identification using a MIMO array. *Electronics* **2018**, *7*, 37. [[CrossRef](#)]
50. Zhu, A.; Qi, X.; Fan, T.; Gu, Z.; Lv, Q.; Ye, D.; Huangfu, J.; Sun, Y.; Zhu, W.; Ran, L. Indoor localization for passive moving objects based on a redundant SIMO radar sensor. *IEEE Trans. Emerg. Sel. Topics Circuits Syst.* **2018**, *8*, 271–279. [[CrossRef](#)]
51. Nosrati, M.; Shahsavar, S.; Lee, S.; Wang, H.; Tavassolian, N. A concurrent dual-beam phased-array Doppler radar using MIMO beamforming techniques for short-range vital-signs monitoring. *IEEE Trans. Antennas Propag.* **2019**, *67*, 2390–2404. [[CrossRef](#)]
52. Wang, S.; Kueppers, S.; Cetinkaya, H.; Herschel, R. 3D localization and vital sign detection of human subjects with a 120 GHz MIMO radar. In Proceedings of the International Radar Symposium, Ulm, Germany, 26–28 June 2019; pp. 1–6. [[CrossRef](#)]
53. Sakamoto, T. Noncontact measurement of human vital signs during sleep using low-power millimeter-wave ultrawideband MIMO array radar. In Proceedings of the IEEE MTT-S International Microwave Biomedical Conference, Nanjing, China, 6–8 May 2019; pp. 1–4. [[CrossRef](#)]
54. Xiong, J.; Zhang, H.; Hong, H.; Zhao, H.; Zhu, X.; Li, C. Multi-target vital signs detection using SIMO continuous-wave radar with DBF technique. In Proceedings of the IEEE Radio and Wireless Symposium, San Antonio, TX, USA, 26–29 January 2020; pp. 194–196. [[CrossRef](#)]
55. Sacco, G.; Pisa, S. A MIMO radar for vital signs recording. In Proceedings of the Photonics & Electromagnetics Research Symposium, Rome, Italy, 17–20 June 2019; pp. 387–393. [[CrossRef](#)]



© 2020 by the authors. Licensee MDPI, Basel, Switzerland. This article is an open access article distributed under the terms and conditions of the Creative Commons Attribution (CC BY) license (<http://creativecommons.org/licenses/by/4.0/>).